AIAA JOURNAL
Vol. 49, No. 10, October 2011

# New Numerical Procedure for Impedance Eduction in Ducts Containing Mean Flow

W. R. Watson* and M. G. Jones†
*NASA Langley Research Center, Hampton, Virginia 23681-2199, USA*

DOI: 10.2514/1.J050317

**A new impedance eduction method is presented and validated against a benchmark method, and the effects of measurement uncertainty errors on the impedances educed with this new method are assessed. Unique features of the new method include the following: 1) the upstream and downstream boundary conditions contain higher-order duct modes, 2) the impedance spectra of unique nonuniform test liners on opposite walls may be educed simultaneously, and 3) the measured data for the impedance eduction are acquired only at the source and duct termination planes. The validation exercise is performed with a rigid-wall insert and a conventional liner over a range of frequencies and flow Mach numbers in the NASA Langley Research Center's grazing flow impedance tube. The primary conclusions of the study are that the impedance spectra of the rigid-wall insert and the conventional liner that were educed from the new method are in very good agreement with those that were educed by using the benchmark method. However, the effects of measurement uncertainty on the educed impedance are greater at the lower frequencies and the higher Mach numbers for the new method. All indications are that this occurs because the new method 1) uses significantly less data to perform the impedance eduction than the benchmark and 2) is currently based on a rather crude approximation to the measured pressure gradient, which is more sensitive to the refractive effects of the boundary layer than the measured lower-wall pressure that is required in the benchmark method.**



## Nomenclature

| | | |
|---|---|---|
| $[A]$, $[\bar{A}]$ | = | global stiffness matrices with and without source effects |
| $a$, $b$ | = | length and height of a finite element |
| $B_{m,n}$ | = | complex coefficients for mode $(m, n)$ |
| $C$, $S$ | = | normalized conductance and susceptance of wall liner $r$ |
| $c_0$, $M_0$, $\rho_0$ | = | speed of sound, uniform-flow Mach number, mean static density |
| $\{D\}$, $\{X\}$ | = | column vectors used in optimization algorithm |
| $\{F\}$, $\{\Phi\}$ | = | right-hand-side force vector, global vector of unknown nodal parameters |
| $f$, $\omega$, $t$ | = | source frequency, circular harmonic frequency, dimensional time |
| $f_q$, $N_q$ | = | two-dimensional and three-dimensional cubic polynomial basis functions |
| $H$, $L$, $W$ | = | height, length, and width of three-dimensional duct |
| $[HM]$, $[\overline{HM}]$ | = | positive definite matrices used to update the inverse Hessian matrix |
| $[I, J]$ | = | the finite element in the $I$th column and $J$th row of the two-dimensional grid |
| $i$, $\Phi_q$ | = | unit imaginary number, the unknown nodal parameters for an element |
| $k$, $K$ | = | free-space wave number, axial wave number |
| $L_1$, $L_2$ | = | locations of leading and trailing edges of test liners |
| $M$, $N$ | = | number of grid lines in the $x$ and the $z$ direction |
| $NH$, $NV$ | = | number of modes in the horizontal and vertical directions |
| $p$, $P$ | = | 3-D acoustic pressure field; quasi-three-dimensional acoustic pressure field |
| $R$, $\phi(\{X\})$ | = | field residual for governing differential equation. objective function |
| $t_{\text{fac}}$, $\lvert\ \rvert$ | = | $t$-factor for uncertainty analysis, absolute value of a complex quantity |
| $x$, $y$, $z$ | = | vertical coordinate, horizontal coordinate; axial coordinate |
| $\{Y\}$ | = | column vector used in optimization algorithm |
| $\beta_1(z)$, $\beta_2(z)$ | = | normalized acoustic admittance of lower and upper walls |
| $\zeta_1(z)$, $\zeta_2(z)$ | = | normalized acoustic impedance of lower- and upper-wall test liners |
| $\theta_1$, $\theta_2$ | = | normalized acoustic resistance of lower- and upper-wall test liners |
| $\sigma$, $\tau$, $\nabla$ | = | standard deviation, tolerance for the optimization algorithm; gradient vector |
| $\chi_1$, $\chi_2$ | = | normalized acoustic reactance of lower- and upper-wall test liners |

*Subscripts*

| | | |
|---|---|---|
| CI | = | 95% confidence interval |
| $m$, $n$ | = | horizontal mode order, vertical mode order |
| $me$, $ms$ | = | termination-plane quantity, source-plane quantity |
| $me1$, $ms1$ | = | axial station just before termination -plane, axial station just after source plane |
| $q$, $I$, $J$ | = | basis function counter, axial grid line counter, vertical grid line counter |

*Superscripts*

| | | |
|---|---|---|
| Exact, Mean | = | exact quantity; mean value |
| FEM, Meas | = | a finite element computed quantity, a measured quantity |
| WPM, PGM | = | wall pressure method, pressure gradient method |

Presented as Paper 2009-3236 at the 15th AIAA/CEAS Aeroacoustics conference, Miami, FL, 11–13 May 2009; received 2 November 2009; revision received 16 December 2010; accepted for publication 13 March 2011. 

*Senior Research Scientist, Research and Technology Directorate, Computational Aerosciences Branch, Liner Physics Group. Associate Fellow AIAA.

†Senior Research Scientist, Research and Technology Directorate, Structural Acoustics Branch, Head of the Liner Physics Group. Associate Fellow AIAA.

$r, T$ = iteration counter for optimization algorithm, matrix/vector transpose
$*, +$ = complex conjugate and right-moving mode

## I. Introduction

INCREASINGLY stringent international noise constraints have resulted in continued emphasis on the development of improved technologies to reduce the overall level of fan noise that is radiated to communities that surround airports. Local-reacting acoustic liners mounted in the aircraft engine nacelles currently provide significant fan-noise reduction, but further optimization is required to increase their noise reduction capacity. The critical intrinsic parameter that is used in this optimization is the local-reacting acoustic impedance of the liner. Therefore, an accurate knowledge of this quantity is critical for the design of quieter aircraft. Further, the local-reacting impedance of a nacelle liner is defined as the ratio of the acoustic pressure to the normal component of acoustic particle velocity at the surface of the liner. Direct measurement of both parameters at the liner surface is problematic at best. Instead, a number of indirect methods have been developed to determine the local-reacting acoustic impedance of a liner. Four such methods are briefly reviewed in this Introduction.

The first indirect method for determining the local-reacting liner impedance is the standing-wave method [1]. For this method, a continuous trace of sound pressure level versus distance from the sample surface is used to determine the standing-wave pattern, which in turn is used to determine the liner impedance. Improvements in instrumentation and analysis tools led to a simpler two-microphone method [2–5], in which two microphones flush-mounted in the sidewall of a normal-incidence impedance tube are used to sample the standing-wave pattern at two fixed locations. This method greatly reduces the data acquisition time that is required for measurement of the liner impedance. However, both methods are only suitable for evaluation of liners in the absence of mean flow. The third method is the in situ method [6], which relies on acoustic pressure measurements at the facesheet and backplate of the sample. This method is simple to implement and has been used extensively to determine the impedance of acoustic liners both with and without flow. However, it yields only local information about the liner impedance and is subject to microphone installation effects that become more severe as flow Mach number increases.

The acoustic performance of sound-absorbing materials in aircraft engine nacelles varies significantly with grazing flow [7]. This variability is attributed to the convective and refractive effects of the grazing flow and to flow-induced changes in the liner impedance. Although the two-microphone method is used almost universally for measuring acoustic impedance in the absence of grazing flow, the physical nature of the normal-incidence tube (i.e., closed at the sample end) does not allow the method to be applied in environments with grazing flow and grazing-incidence sound. Instead, the effects of grazing flow and grazing-incidence sound on the liner impedance are commonly determined in a waveguide that is specifically designed for this purpose [8–11].

Over the last three decades, NASA Langley Research Center (LaRC) has also developed a number of test rigs for the evaluation of local-reacting acoustic liners in the presence of grazing flow. The most notable of these are the grazing flow impedance tube (GFIT) [12] and the curved-duct test rig (CDTR) [13]. The remainder of this Introduction discusses waveguide methods, which are used in combination with the GFIT to determine the impedance of local-reacting liners. Because the waveguide methods require the impedance to be educed from other measurements, these processes are commonly described as impedance eduction methods. They involve solving a convected (or sheared flow) wave equation, as well as taking acoustic measurements away from the liner surface, and can be applied for an infinite or a finite waveguide.

The infinite waveguide method, often referred to as the single-mode method [14], involves measuring the axial wave number for a single predominant mode in a waveguide that is lined with acoustic material. The measured axial wave number for the mode is used in conjunction with both the solution to the convected (or sheared flow) wave equation and the local-reacting wall impedance boundary condition to educe the impedance of the liner [7,15–17]. The single-mode method is applicable in a very straightforward manner to a situation for which a single progressive mode propagates over the axial extent of a finite length liner that is mounted in the wall of a waveguide. This method breaks down when the end effects that result from impedance discontinuities at the leading and trailing edges of the liner propagate over the extent of the liner or when more than one mode is dominant. The finite waveguide method has been developed to handle these conditions.

The finite waveguide method for impedance eduction was first proposed in the mid-1990s [18]. This method has evolved from a no-flow model [18] to a uniform-flow model [19] to a sheared-flow model [20]. The original methodology [19] has been extensively reported and validated [14,21–25]. Problems with the method occur when the objective function is flat (e.g., near antiresonance). Also, some accuracy issues with the measured exit impedance have been reported, and a proper choice for the uniform-flow Mach number is questionable at higher flow Mach numbers where boundary-layer effects are more important. Reformulation of the equations to use an exit-pressure condition [25] resolved the first of these issues. Also, earlier results [20] demonstrated that including the boundary-layer effects in the solution improved the results at higher Mach numbers. As an alternate approach, Eversman and Gallman [26] developed an extended search procedure that used the original method [19] and contained the exit impedance and uniform-flow Mach number as part of the search process. The extended search procedure improved the match with the measured data at the higher Mach number but required considerably more computations.

Because of the small cross-sectional dimensions of the GFIT ($0.05 \times 0.06$ m), the flow profile is dominated by the boundary layer. However, a recent study [27] based on the data [23] that were acquired in the predecessor to the GFIT (a 0.05-m $\times$ 0.05-m waveguide) found minimal differences between impedance spectra that were educed with uniform and shear flow models. As will be discussed later, the purpose of the current study is to validate a new impedance eduction method that is suitable for implementation with data that are acquired in the CDTR, a test rig with cross-sectional dimensions of $0.15$ m $\times$ $0.38$ m. This increased duct size supports a uniform core flow over a much larger portion of the cross section. Therefore, the new method proposed here retains the assumption of uniform flow.

Another concern regarding impedance eduction methods is the use of the Myers's wall impedance boundary condition [28]. Several recent studies have investigated the potential for a hydrodynamic instability when this boundary condition is used at the liner surface. An excellent review of this issue is provided by Rienstra and Darau [29]. One study was found that provides experimental evidence of this instability [30], based on data that were measured with a ceramic liner with rectangular channels. However, no experimental evidence of this hydrodynamic instability has been presented with conventional liners or with the ceramic liner (with round channels) that is used by NASA. Thus, one can reasonably assume that if the instability is indeed real, the test conditions that are used at NASA do not excite the instability. Also, careful examination of the measured data and numerical solutions used in this paper fully support this conclusion.

In the last decade, a number of additional finite waveguide impedance eduction models have appeared in the literature [8,27,31–35]. A detail discussion of these methods is beyond the scope of this paper. However, these methods assume that hard-wall sections exist upstream and downstream of the test liner and each have advantages and disadvantages depending on the available computer resources, the waveguide geometry and instrumentation, and the choice of eduction data. Throughout this paper, the term "eduction data" is defined as the measured data (within the waveguide) that is required to educe the unknown impedance.

One of the current NASA LaRC goals is to implement impedance eduction using the CDTR. This rig was initially designed [13] as a test bed to quantify the performance of current liner designs and to develop new concepts for efficient duct liner treatments in the

presence of grazing flow and wall curvature. The CDTR offers a number of attractive features:

1) Its cross section is close to the size of an aft bypass duct of a full-scale engine.

2) Flow profiles acquired in the CDTR are nearly uniform over a large portion of the duct.

3) Acoustic energy in higher-order duct modes can be controlled.

4) The effects of wall curvature can be evaluated.

However, careful review indicates that none of the aforementioned impedance eduction methods can be applied to data that are acquired in the CDTR. This occurs for three primary reasons:

1) The aforementioned methods use multimodal analysis techniques in the liner test section [8,27,31–35] and these techniques are generally not applicable within the curved portion of a lined duct.

2) Many of the methods assume that only plane waves are cut on in the hard-wall sections of the duct [8,27,31–33].

3) Most of the impedance eduction methods require eduction data from within the liner test section [8,19,27,33,34], while the goal of the current method is to rely solely on data that are acquired in the hard-wall sections outside the liner test section.

In two recent papers [36,37], the authors present a new impedance eduction method that is more suited for implementation with the CDTR:

1) The method requires eduction data from only the source and termination planes of the duct.

2) It does not depend on multimodal analysis (i.e., it is extendable to curved ducts such as the CDTR).

3) It is applicable to liner test sections where the opposite wall contains another liner (e.g., the CDTR).

4) It is applicable to ducts with higher-order cuton modes (e.g., the CDTR).

The primary purpose of this paper is to validate this new impedance eduction method with measured data from both a rigid-wall insert and a conventional test liner over a range of flow Mach numbers and source frequencies. Data acquired in the GFIT are used as input for the validation exercise, and the impedance spectra that are educed from the method are compared with those from a well-established benchmark method [19]. In addition, the effects of measurement uncertainty on the new methodology are also assessed.

## II. Problem Description

Figure 1 shows a schematic of the duct configuration for which impedance eduction is desired. The upper and lower walls of the duct contain test liners; hard-wall sections exist upstream and downstream of the test liners; and the left and right sidewalls are rigid. A right-hand Cartesian coordinate system is used in which the axial, vertical, and horizontal directions are denoted by $z$, $x$, and $y$, respectively. The duct has length $L$, uniform height $H$, and uniform width $W$. Provisions are made later to allow for a nonuniform cross-sectional area distribution in the liner test section. Such a nonuniform area distribution exists, for example, when the LaRC CDTR is operated in a curved configuration.

As usual, all transients in the duct are assumed to have been dissipated away or to have propagated out of the solution domain, so that acoustic disturbances are assumed to be at steady state with a harmonic time dependence of the form $e^{i\omega t}$. The source and duct termination planes are located at $z = 0$ and $z = L$, respectively, and the origin of the coordinate system is the lower left corner of the source plane, as illustrated in Fig. 1. Both test liners are assumed to be locally reacting (i.e., acoustic waves propagate through them normal to the liner surface) and each liner is assumed to lie between the axial locations, $L_1 \le z \le L_2$; outside this region, the upper and lower walls are assumed to be rigid. The normalized acoustic impedances of the lower- and upper-wall liners are denoted by $\zeta_1(z)$ and $\zeta_2(z)$, respectively, so that the impedances of these liners may vary with axial location. Further, all impedances are normalized with the characteristic impedance $\rho_0 c_0$ of the air in the duct.

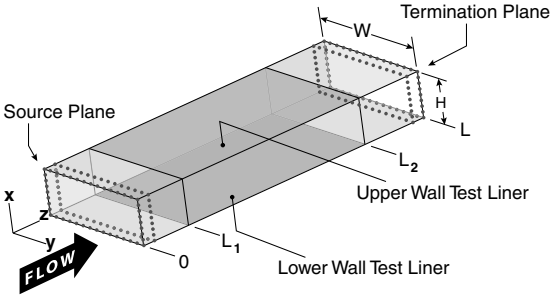


**Fig. 1 Schematic of three-dimensional rectangular duct with upper- and lower-wall test liners.**

A subsonic mean flowfield exists from left to right along the axis of the duct, as shown in Fig. 1, and the Mach number of the mean flowfield is denoted by the symbol $M_0$. However, the boundary layer that is generated by the flow is assumed to be thin, so that the uniform-flow assumption is reasonable. [In the Introduction section, we provided the rationale for making the uniform-flow assumption even in a duct with small cross-sectional dimensions (i.e., the GFIT).] Further, the duct configuration is a model of an aft-fan duct (i.e., sound and flow are in the same direction). Alternatively, inlet duct modeling (i.e., flow and sound are directed in opposite directions) is achieved by reversing the sign on the Mach number. The problem at hand is to educe the unknown acoustic impedances of the test liners in the presence of the uniformly flowing fluid and higher-order duct modes.

## III. Governing Differential Equation and Boundary Conditions

The acoustic pressure field that propagates in the duct that is depicted in Fig. 1 satisfies the convected Helmholtz equation:

$$(1 - M_0^2)\frac{\partial^2 p}{\partial z^2} + \frac{\partial^2 p}{\partial x^2} + \frac{\partial^2 p}{\partial y^2} - 2ikM_0\frac{\partial p}{\partial z} + k^2 p = 0, \qquad k = \frac{\omega}{c_0} \tag{1}$$

Assumptions that are made in the derivation of Eq. (1) can be found in standard aeroacoustics textbooks [38] and are not discussed further herein. The solution that satisfies the rigid-wall boundary conditions along the sidewalls is of the form

$$p(z, x, y) = \sum_{m=0}^{NH-1} P_m(z, x)\cos\left(\frac{m\pi y}{W}\right) \tag{2}$$

where the number of horizontal modes, $NH$, is chosen to be large enough to include both the cuton modes that carry acoustic energy and a sufficient number of cutoff modes so that the series expansion represents a complete set. As usual, the cutoff modes are defined as those modes that are attenuated as they propagate along a hard-wall section of the duct. Because the solution in the horizontal dimension is separable, each $P_m$ is a quasi-3-D solution and satisfies a modified, convected Helmholtz equation of the form

$$(1 - M_0^2)\frac{\partial^2 P_m}{\partial z^2} + \frac{\partial^2 P_m}{\partial x^2} - 2ikM_0\frac{\partial P_m}{\partial z} + \left[k^2 - \left(\frac{m\pi}{W}\right)^2\right]P_m = 0 \tag{3}$$

The wall impedance boundary condition for a locally reacting liner has been discussed in detail by Myers [28], and the rationale for the continued use of this boundary condition is given in the Introduction. For the upper wall, the Myers locally reacting boundary condition is

$$-\frac{\partial P_m}{\partial x} = ik\left(\frac{P_m}{\zeta_2}\right) + 2M_0\frac{\partial}{\partial z}\left(\frac{P_m}{\zeta_2}\right) + \frac{M_0^2}{ik}\frac{\partial^2}{\partial z^2}\left(\frac{P_m}{\zeta_2}\right) \tag{4}$$

and the wall impedance boundary condition of the lower wall has a similar form:

$$\frac{\partial P_m}{\partial x} = ik\left(\frac{P_m}{\zeta_1}\right) + 2M_0\frac{\partial}{\partial z}\left(\frac{P_m}{\zeta_1}\right) + \frac{M_0^2}{ik}\frac{\partial^2}{\partial z^2}\left(\frac{P_m}{\zeta_1}\right) \tag{5}$$

Equations (4) and (5) are also used along the rigid-wall portion of the upper- and lower-wall, but the admittance function (i.e., the reciprocal of the impedance function) is set to zero along this portions of the wall (i.e., $\beta_1 = 1/\zeta_1 = 0.0 + 0.0i$ and $\beta_2 = 1/\zeta_2 = 0.0 + 0.0i$).

Two arrays of microphones are flush-mounted strategically around the circumference of the duct at the source plane (i.e., $z = z_1 = 0$) and at a second axial station ($z = z_2$) just downstream of the source plane, as depicted in Fig. 1. The location of each microphone in the first and second microphone array is assumed to be at the same vertical and horizontal location, $(x_J, y_k)$, and the axial location, $z = z_2$, is assumed to be sufficiently close to the source plane so that the acoustic pressure gradient normal to the source boundary can be accurately resolved by using the forward difference expression:

$$\frac{\partial P_m^{\text{Meas}}(0, x_J)}{\partial z} = \frac{P_{ms1}^{\text{Meas}}(x_J) - P_{ms}^{\text{Meas}}(x_J)}{(z_2 - z_1)} \tag{6}$$

Here, $x_J$ is the transverse location of the microphone along the rigid sidewall, and the measured acoustic pressure field is assumed to be decomposed into hard-wall duct modes, $m$, in the horizontal direction. A similar expression for the gradient that is normal to the exit or duct termination plane is developed by using the backward difference expression

$$\frac{\partial P_m^{\text{Meas}}(L, x_J)}{\partial z} = \frac{P_{me}^{\text{Meas}}(x_J) - P_{me1}^{\text{Meas}}(x_J)}{(z_N - z_{N-1})} \tag{7}$$

where $z_N = L$ and $z_{N-1}$ are the axial locations of the exit plane and the microphone array just upstream of the exit plane, respectively, (see Fig. 1).

The measured acoustic pressure profile is used as the source- and exit-plane boundary condition for each horizontal mode $m$:

$$P_m(0, x_J) = P_{ms}^{\text{Meas}}(x_J) \tag{8}$$

$$P_m(L, x_J) = P_{me}^{\text{Meas}}(x_J) \tag{9}$$

Note that a termination-plane boundary condition that uses exit impedance could be derived. However, a measurement of exit impedance may not be sufficiently accurate for the impedance eduction, and an exit-pressure boundary condition yields more stable and consistent results [25]. Therefore, the current formulation incorporates the exit acoustic pressure condition [Eq. (9)] as the termination-plane boundary condition. When the liner impedance functions $\zeta_1$ and $\zeta_2$ are known, Eqs. (3–5), (8), and (9) constitute a well-posed boundary-value problem that can be solved to obtain the acoustic pressure field and its derivatives. The difficulty here is that these impedance functions are not known; thus, this boundary-value problem is ill-posed. To achieve a well-posed boundary-value problem, initial guesses for the impedance functions are provided, and these initial guesses are iteratively updated until the acoustic pressure gradients that are normal to the source and duct termination planes match those from an experimental measurement. We demonstrate later that the impedance functions that reproduce these measurements are the unknown impedance functions of the test liners. However, the acoustic pressure gradients that are normal to the source and duct termination planes do not have closed-form solutions for comparison. Consequently, they are computed numerically by using a finite element method (FEM). A few of the most important details in regard to the FEM are given in the following section.

## IV. Finite Element Solution for the Acoustic Field

In the duct that is depicted in Fig. 1, a grid is used that consists of $N$ and $M$ evenly spaced grid lines in the $z$ and $x$ directions of the duct,

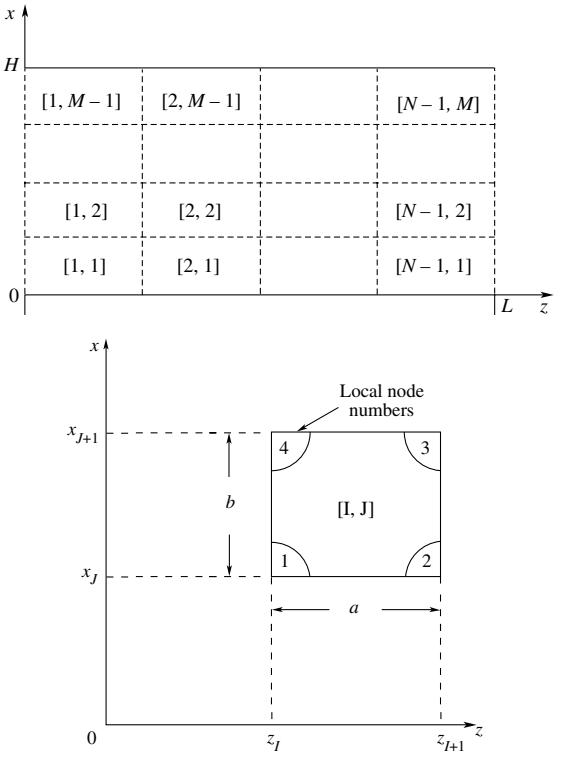


**Fig. 2 Finite element discretization and node-numbering system.**

respectively. The $N$ grid lines in the $z$ direction are assumed to be located at the axial locations $z = z_1, z = z_2, \ldots, z = z_N$. Similarly, the $M$ evenly spaced grid lines in the $x$ direction are assumed to be located at $x = x_1, x = x_2, \ldots, x = x_M$ (where $x_1 = 0$ and $x_M = H$). Thus, $N - 1$ columns and $M - 1$ rows of elements are located in the duct, as shown in the upper part of Fig. 2. Therefore, we conveniently use a double-subscript notation $[I, J]$ to locate the element in the $I$th column and the $J$th row of the grid, where $I = 1, 2, 3, \ldots, N - 1$ and $J = 1, 2, 3 \ldots, M - 1$. A typical rectangular element $[I, J]$ consists of four local node numbers that are labeled 1, 2, 3, and 4, respectively, as shown in the bottom part of Fig. 2. The objective is to obtain the unknown acoustic pressure and its derivatives at the nodes of each of the $(M - 1)(N - 1)$ rectangular elements. This is achieved by using a conventional Galerkin FEM to minimize the field residual error, which is defined as

$$R = (1 - M_0^2)\frac{\partial^2 P_m}{\partial z^2} + \frac{\partial^2 P_m}{\partial x^2} - 2ikM_0\frac{\partial P_m}{\partial z} + \left[k^2 - \left(\frac{m\pi}{W}\right)^2\right]P_m \tag{10}$$

Within each rectangular element $[I, J]$ the quasi-3-D acoustic pressure field $P_m$ is approximated as a polynomial expression. This polynomial expression is chosen based on the following criteria:

1) The normal gradients of the acoustic pressure at the source and the duct termination planes are needed for impedance eduction; therefore, they must be highly accurate.

2) The numerical differentiation of the acoustic pressure field to obtain the pressure gradient must be avoided, which reduces the error in the eduction procedure. Therefore, the pressure gradients are used as nodal degrees of freedom in the FEM.

A polynomial that satisfies the above criteria in each element and that is consistent with the continuity and convergence requirements of the FEM is

$$P_m(z, x) = \sum_{q=1}^{q=16} N_q(z, x)\Phi_q, \qquad z_I \le z \le z_{I+1} \qquad x_J \le z \le x_{J+1} \tag{11}$$

where the unknown nodal coefficients $\Phi_q$ are the values of

$$P_m, \qquad \frac{\partial P_m}{\partial z}, \qquad \frac{\partial P_m}{\partial x}, \qquad \frac{\partial^2 P_m}{\partial z \partial x}$$

at the four nodes of the element. The basis functions $N_q(z,x)$ are cubic two-dimensional (2-D) polynomials that are nonzero only within the element $[I,J]$. The expressions for these polynomials are rather lengthy and are given in the excellent text by Desai and Abel [39]; therefore, these expressions are not repeated herein. The wall impedance functions are represented in a similar manner along each boundary element as

$$\zeta_1(z) = \zeta_1(z_I) f_1(z) + \frac{\mathrm{d}\zeta_1(z_I)}{\mathrm{d}z} f_2(z) + \zeta_1(z_{I+1}) f_3(z) + \frac{\mathrm{d}\zeta_1(z_{I+1})}{\mathrm{d}z} f_4(z) \tag{12}$$

$$\zeta_2(z) = \zeta_2(z_I) f_1(z) + \frac{\zeta_2(z_I)}{\mathrm{d}z} f_2(z) + \zeta_2(z_{I+1}) f_3(z) + \frac{\mathrm{d}\zeta_2(z_{I+1})}{\mathrm{d}z} f_4(z) \tag{13}$$

where the details of the one-dimensional cubic polynomials $f_q(z)$ are provided by Watson et al. [19] and the nodal coefficients

$$\zeta_1(z_I), \qquad \frac{\mathrm{d}\zeta_1(z_I)}{\mathrm{d}z}, \qquad \zeta_2(z_{I+1}), \qquad \frac{\mathrm{d}\zeta_2(z_{I+1})}{\mathrm{d}z}$$

are assumed to be known. If the liner has a constant impedance, then the impedance coefficients $\zeta_1(z_I)$ and $\zeta_2(z_{I+1})$ may be set to a constant value along the liner and the axial gradients $\mathrm{d}\zeta_1(z_I)/\mathrm{d}z$ and $\mathrm{d}\zeta_2(z_{I+1})/\mathrm{d}z$ set to zero. This will reduce the amount of computation but is not a requirement for the new eduction method.

The field error in the duct is now minimized by requiring that it be orthogonal to each basis function $N_q(z,x)$. Contributions to the minimization of the field-error function from a typical finite element are of the form

$$\int_{[I,J]} R N_q \, \mathrm{d}z \, \mathrm{d}x \tag{14}$$

The wall impedance boundary conditions (4) and (5) are implemented in weak form by integrating by parts each second-derivative term in the integrand of Eq. (14) and substituting the wall impedance boundary conditions. The contribution to the minimization of the field error and wall impedance boundary conditions for a typical element $[I,J]$ is expressed in matrix form as

$$\int_{[I,J]} R N_q \, \mathrm{d}z \, \mathrm{d}x = [\bar{A}^{[I,J]}]\{\Phi^{[I,J]}\} \tag{15}$$

where the coefficients in the element stiffness matrix $[\bar{A}^{[I,J]}]$ are computed in closed form. The assembly of the global matrix equations from the local element stiffness matrices is a basic procedure in the FEM. Appropriate shifting of rows and columns is all that is required to add the local element stiffness matrix $[\bar{A}^{[I,J]}]$ directly into the global stiffness matrix $[\bar{A}]$. This results in a matrix equation of the form

$$[\bar{A}]\{\Phi\} = \{0\} \tag{16}$$

where $\{\Phi\}$ is partitioned as follows:

$$\{\Phi\} = \begin{Bmatrix} \{P_1\} \\ \{P_2\} \\ \{P_3\} \\ \vdots \\ \{P_N\} \end{Bmatrix}, \qquad \{P_I\} = \begin{Bmatrix} P_m(z_I, x_1) \\ \frac{P_m(z_I,x_1)}{\partial z} \\ \frac{\partial P_m(z_I,x_1)}{\partial x} \\ \frac{\partial^2 P_m(z_I,x_1)}{\partial z \partial x} \\ P_m(z_I, x_2) \\ \frac{P_m(z_I,x_2)}{\partial z} \\ \vdots \\ \frac{\partial^2 P_m(z_I,x_M)}{\partial z \partial x} \end{Bmatrix} \tag{17}$$

Equations (16) are a set of linear algebraic equations that minimize the residual error in the duct while satisfying the wall impedance boundary conditions in weak form. Solutions to Eqs. (16) do not, however, satisfy the source- and termination-plane boundary conditions. These two conditions are satisfied by constraining the nodal degrees of freedom $\Phi_q$ in the trial solution that is given in Eq. (11). Thus, for each element along the source boundary, the following constraints are imposed on these local degrees of freedom:

$$\begin{Bmatrix} \Phi_1 \\ \Phi_3 \\ \Phi_{13} \\ \Phi_{15} \end{Bmatrix} = \begin{Bmatrix} P_{ms}^{\mathrm{Meas}}(x_J) \\ \frac{\mathrm{d}P_{ms}^{\mathrm{Meas}}(x_J)}{\mathrm{d}x} \\ P_{ms}^{\mathrm{Meas}}(x_{J+1}) \\ \frac{\mathrm{d}P_{ms}^{\mathrm{Meas}}(x_{J+1})}{\mathrm{d}x} \end{Bmatrix} \tag{18}$$

These constraints are imposed on each degree of freedom by giving a null value to each coefficient in the row of $[\bar{A}]$ that corresponds to each known degree of freedom, with the exception of the diagonal element, which is made equal to unity; the known value for the degree of freedom is inserted into the right-hand-side null vector $\{0\}$ [39]. Similarly, for each element along the duct termination plane the following constraints are imposed on the local degrees of freedom:

$$\begin{Bmatrix} \Phi_5 \\ \Phi_7 \\ \Phi_9 \\ \Phi_{11} \end{Bmatrix} = \begin{Bmatrix} P_{me}^{\mathrm{Meas}}(x_J) \\ \frac{\mathrm{d}P_{me}^{\mathrm{Meas}}(x_J)}{\mathrm{d}x} \\ P_{me}^{\mathrm{Meas}}(x_{J+1}) \\ \frac{\mathrm{d}P_{me}^{\mathrm{Meas}}(x_{J+1})}{\mathrm{d}x} \end{Bmatrix} \tag{19}$$

Imposing these constraints (18) and (19) on Eq. (16) leads to a modified system of linear algebraic equations that satisfy the source- and termination-plane boundary conditions. This modified system is of the form

$$[A]\{\Phi\} = \{F\} \tag{20}$$

where $\{F\}$ contains the effects of the sound source and the exit-pressure boundary conditions. Equations (20) make up the system of linear algebraic equations that are solved to obtain the acoustic pressure and its derivatives in the duct for specified wall impedance functions. The solution is obtained by using the software package Pardiso[‡] (a state-of-the-art parallel sparse solver with equation reordering and iterative refinement). The Pardiso software returns the solution for the acoustic pressure field and its derivatives at the $MN$ nodes of the duct. The procedure that is described in the following section uses these derivatives to educe the unknown impedance functions.

## V. Impedance Eduction Procedure

In this section, a numerical procedure is developed to educe the unknown impedances of the test liners by using the FEM solution that is obtained from Eq. (20) and the solution that is obtained from the measured data [Eqs. (6) and (7)]. The boundary-value problem that is described by Eqs. (3–5), (8), and (9) is well-posed; thus, the solutions for the acoustic pressure field and its gradient are unique. Therefore, the numerical solution to Eq. (20) will give unique values for these two fields for each set of the impedance functions [i.e., $\zeta_1(z)$

[‡]Data available online at http://developer.intel.com [retrieved April 2009].

and $\zeta_2(z)$]. Additionally, the measured values for these two fields at the source and duct termination planes [Eqs. (6) and (7)] provide solutions for these two fields. If the impedances of the test liners are properly chosen, then the solutions from the finite element solution and the measured data for the acoustic pressure gradients that are normal to the source and duct termination planes will match. This means that the following equations will be satisfied:

$$\frac{\partial P_m^{\text{Meas}}(0, x_J)}{\partial z} - \frac{\partial P_m^{\text{FEM}}(0, x_J)}{\partial z} = 0 \qquad (J = 1, 2, 3, \ldots, M) \quad (21)$$

$$\frac{\partial P_m^{\text{Meas}}(L, x_J)}{\partial z} - \frac{\partial P_m^{\text{FEM}}(L, x_J)}{\partial z} = 0 \qquad (J = 1, 2, 3, \ldots, M) \quad (22)$$

Equations (20) may be solved to obtain the gradient of the acoustic pressure field in the duct for the initial values of the wall impedance functions $\zeta_1(z)$ and $\zeta_2(z)$, and these impedance functions may be iteratively updated until the solutions for the pressure gradient that are computed from Eq. (20) match the measured data [see Eqs. (6) and (7)] to within some tolerance.

However, the proposed iterative procedure must be automated so that each new update to the impedance functions brings the FEM solution closer to that obtained from the measured data. An automated search procedure is therefore implemented with the use of an optimization algorithm. The objective, or cost function, for the optimization is a real-valued function of the normalized resistance $\theta$ and the normalized reactance $\chi$ of the test liners (i.e., $\zeta_1 = \theta_1 + i\chi_1$ and $\zeta_2 = \theta_2 + i\chi_2$). The objective function $\phi$ for the optimization algorithm is defined as

$$\phi(\{X\}) = \sum_{J=1}^{M} \left[ \left| \frac{\partial P_m^{\text{Meas}}(0, x_J)}{\partial z} - \frac{\partial P_m^{\text{FEM}}(0, x_J)}{\partial z} \right| + \left| \frac{\partial P_m^{\text{Meas}}(L, x_J)}{\partial z} - \frac{\partial P_m^{\text{FEM}}(L, x_J)}{\partial z} \right| \right] \quad (23)$$

$$\{X\}^T = \{\theta_1, \chi_1, \theta_2, \chi_2\} \quad (24)$$

Note the following:

1) The objective function is real and non-negative (i.e., $\phi(\{X\}) \geq 0$).

2) The global minimum of the objective function $\phi(\{X\}) = 0$ occurs when the gradient of the acoustic pressure field matches that of the measured data.

Therefore, the normalized resistance and reactance functions that minimize $\phi(\{X\})$ are those that correspond to the test liners. The optimization algorithm returns the solution vector $\{X\}$ that minimizes the objective function $\phi(\{X\})$.

The optimization algorithm that is used in this paper is a modification of the Davidon–Fletcher–Powell (DFP) optimization algorithm. The DFP algorithm is a technique for finding the minimum of an objective function such as $\phi(\{X\})$ that is a differential function of several variables. The DFP optimization algorithm was first proposed by Davidon [40] and was later reformulated and popularized by Fletcher and Powell [41]. When given a starting position $\{X^{(r)}\}$ and a symmetric positive definite matrix $[HM^{(r)}]$, the DFP algorithm is an iterative procedure that searches along a line from $\{X^{(r)}\}$ in a direction $\{D^{(r)}\}$ to a new point $\{X^{(r+1)}\}$ with a decreased function value. The DFP algorithm, as it is used in this research, is as follows:

1) Let $[HM^{(r)}]$ be an identity matrix of the same order as $\{X\}$, and let $\{X^{(r)}\}$ be an approximation to $\{X\}$.

2) Compute $\{D^{(r)}\} = -[HM^{(r)}]\nabla\phi(\{X^{(r)}\}$.

3) Locate the minimum of $\phi(\{X^{(r)}\} + \alpha^{(r)}\{D^{(r)}\})$ with respect to $\alpha^{(r)}$ by repeated parabolic interpolation.

4) Update $\{X^{(r)}\}$ for the next iteration by using $\{X^{(r+1)}\} = \{X^{(r)}\} + \alpha^{(r)}\{D^{(r)}\}$.

5) Set $\{Y^{(r)}\}) = \nabla\phi(\{X^{(r+1)}\}) - \nabla\phi(\{X^{(r)}\}$ and $[HM^{(r+1)}] = [HM^{(r)}] + [\overline{HM}^{(r)}]$, where

$$[\overline{HM}^{(r)}] = \alpha^{(r)} \frac{\{D^{(r)}\}\{D^{(r)}\}^T}{\{D^{(r)}\}^T\{Y^{(r)}\}} - \frac{[HM^{(r)}]\{Y^{(r)}\}([HM^{(r)}]\{Y^{(r)}\})^T}{\{Y^{(r)}\}^T[HM^{(r)}]\{Y^{(r)}\}} \quad (25)$$

6) Set $r = r + 1$ and return to step 2.

In the above iterative procedure, an analytical expression for the gradient of $\phi(\{X\})$ (i.e., $\nabla\phi(\{X\})$) is not available. Therefore, the gradient of $\phi(\{X\})$ is computed numerically by using a finite difference approximation that was developed by Stewart [42]. Additionally, the iteration is continued until the following convergence condition is met:

$$\{X^{(r+1)}\} - \{X^{(r)}\} \leq \tau \quad (26)$$

where $\tau$ is the tolerance for each variable in the optimization algorithm.

The DFP algorithm that is used here is modified to accept numerical differentiation (as suggested by Stewart [42]) to compute the gradient and is referred to as the SDFP algorithm in this paper. The SDFP algorithm assumes that $\phi(\{X\})$ can be locally approximated as a quadratic in the region around the optimum point. This optimization method therefore has the disadvantage that it may converge to a local optimum (if one exists) and may become stuck in the portion of the impedance plane where the objective function $\phi(\{X\})$ is extremely flat. However, these shortcomings of the SDFP algorithm are more than mitigated by the fact that the SDFP algorithm converges faster and yields more accurate results than many of its competitors. Because no definitive proof exists that multiple local optima cannot exist during the proposed impedance eduction procedure, the authors advise that multiple initial starting vectors $\{X^{(0)}\}$ be used to strengthen confidence that the global optimum is achieved.

A global-based optimizer, the genetic algorithm (GA), was added to the suite of optimization tools. Although the GA [43] runs in parallel and locates a global optimum, it tends to be much more computationally expensive than the SDFP algorithm because it performs a global search in the complex impedance plane. Note that the GA is used sparingly in this study to spot-check the integrity of the impedances that were educed using the SDFP algorithm. In nearly all cases, the relative difference between the impedances that were educed with the SDFP algorithm and the GA were less than $10^{-1}$. Therefore, only the results from the SDFP algorithm are presented in this paper.

Note that the SDFP algorithm runs only in sequential mode, either constrained or unconstrained. The unconstrained version of the SDFP algorithm sometimes returns negative values for the normalized resistance. A negative resistance is not physically realizable because it corresponds to the production of energy by the liner. One solution to the problem of the unconstrained version of SDFP converging to a negative resistance is to run the constrained version. The constrained version restricts the solution set so that only realizable impedances are educed. For the current study, the normalized resistance was constrained to values between 0 and 10, while the normalized reactance was constrained to values that fall between $-10$ and 10. These values of normalized resistances and reactances encompass the expected range for conventional liners that are used in commercial aircraft. The main concern with the constrained version is the possibility that the SDFP algorithm may get "stuck" on a boundary of the constrained region. For the computations that are presented in this paper, this was observed to occur only rarely and was therefore not considered a significant issue in this work. Unless otherwise stated, the results in this paper were produced with the constrained version of the SDFP algorithm. With only a few exceptions, a stopping criterion (i.e., tolerance) of $1 \times 10^{-8}$ was used to terminate the SDFP algorithm.

## VI. Results and Discussion

The primary purpose of the results that are presented in this section is to validate the new impedance eduction method by comparing the educed impedance from the new method with the educed impedance

from the benchmark method. The first exercise that is presented in this section is performed with the CDTR geometry, which can accept test conditions for which higher-order modes are cut on in the rigid-wall sections of the flow duct. However, impedances are educed using simulated data for which the baseline impedance of the liner is known from prior tests that were conducted in the GFIT, and the eduction data are simulated from the FEM. Essentially, the first exercise that is presented in this section constitutes a consistency check to demonstrate that the new eduction methodology is capable of properly handling the effects of higher-order duct modes. Following this consistency check, the validation is performed using measured data from the GFIT, which is capable of acquiring data for both the new method and the benchmark method. It should be noted that the GFIT geometry is designed to accept test conditions (i.e., Mach numbers and frequencies) for which only planar waves are cuton in rigid-wall sections of the flow duct. Thus, the current validation exercise will not include the effects of sound sources containing high-order duct modes.

### A. Consistency Check

The results of the consistency check are restricted to the geometry of the CDTR for which $L_1 = 0.203$ m, $L_2 = 1.016$ m, $L = 1.219$ m, $W = 0.381$ m, and $H = 0.152$ m. As many as three transverse modes may be cut on for the lowest order horizontal mode in the frequency range of interest (i.e., $0.4 \leq f \leq 3.0$ kHz). Results are obtained for five uniform-flow Mach numbers ($M_0 = 0.0$, 0.1, 0.3, 0.4, and 0.5), and all of the results are computed at standard atmospheric conditions (i.e., $c_0 = 344.28$ m/s and $\rho_0 = 1.20$ kg/m$^3$).

#### 1. *Grid-Refinement Study*

Generally speaking, the computational cost of the impedance eduction procedure grows as the spatial grid increases in density. Therefore, determining the coarsest grid within which the impedance eduction can be performed is prudent. This is achieved by performing a grid-refinement study on four uniformly spaced grids in a rigid-wall duct. The four grids are denoted as G1, G2, G4, and G8. Grid G1 has 49 evenly spaced points ($N = 49$) along the axis of the duct and seven ($M = 7$) evenly spaced points in the vertical direction. The density of the second grid, G2, is obtained by doubling the density (in each coordinate direction) of G1. The third grid, G4, is obtained by doubling the density of G2. Finally, the fourth grid, G8, is obtained by doubling the density of G4. Thus, the G8 grid is 8 times denser (in each coordinate direction) than grid G1 (i.e., $N = 385$ and $M = 49$ on the G8 grid).

The cubic finite element analysis that is used in this work is designed to be fourth-order-accurate on uniform grids. Therefore, the reduction in the residual error on the selected grids is expected to

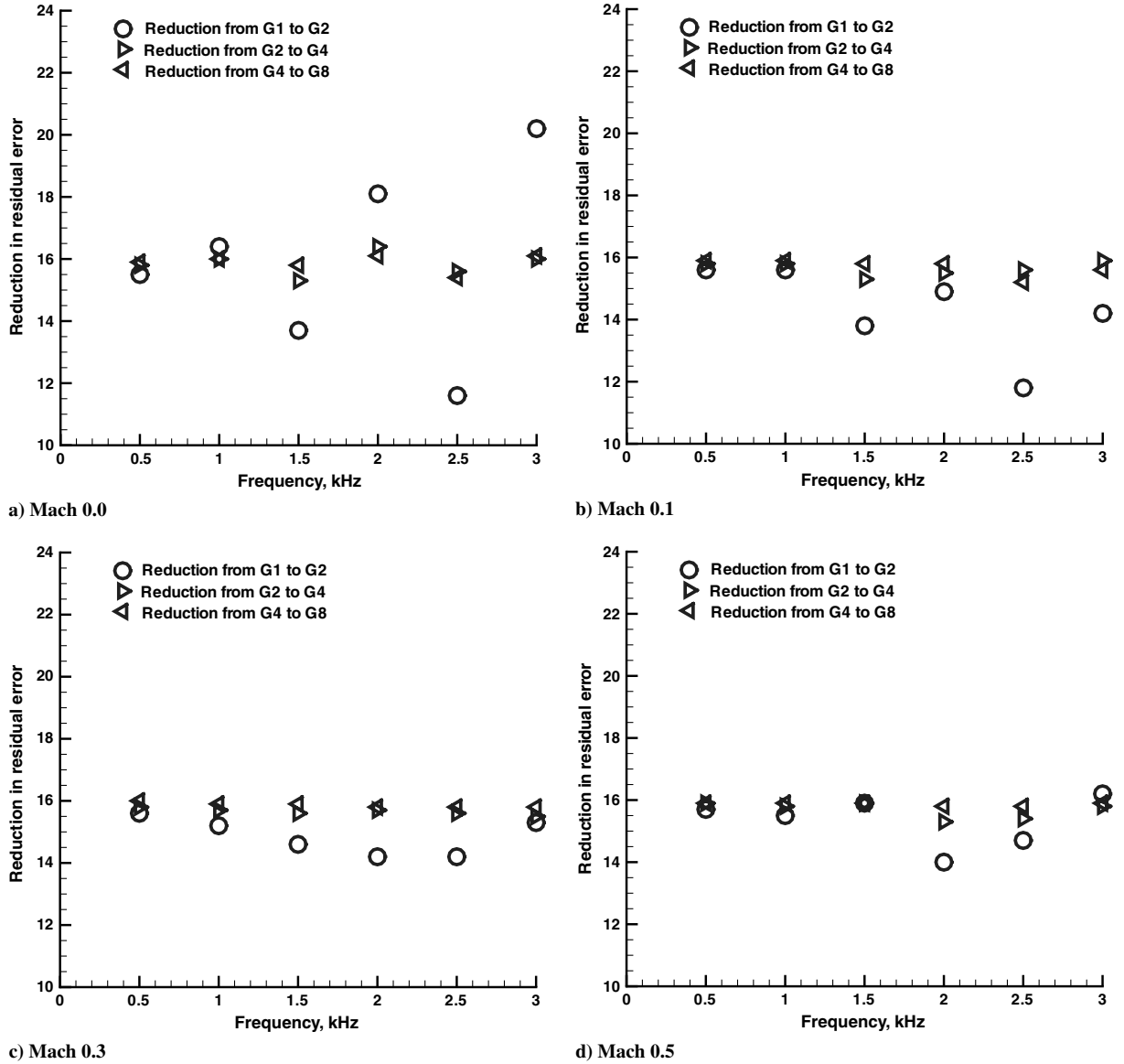


**Fig. 3 Reduction in residual error due to grid doubling for plane-wave source in hard-wall duct.**

approach the design order (i.e., be reduced by a factor of $2^4$ as the grid density is doubled). Further, a significant variability in the reduction of the residual error about the design order is an indication that the chosen grid is too coarse for accurate resolution of the acoustic waves. Figure 3 shows the reduction in residual error that results from a doubling of the grid density as a function of frequency for the four selected Mach numbers ($M_0 = 0.0$, 0.1, 0.3, and 0.5). In Fig. 3, the reduction in the residual error as a result of grid doubling is shown for an outgoing plane wave in a hard-wall duct, so that the exact solution that is used to compute the residual error obtained by the FEM is known:

$$p^{\text{Exact}}(z, x) = B^{+}_{0,0} e^{iK^{+}_{0,0} z} \tag{27}$$

where $B^{+}_{0,0}$ is set to a value of 20 Pa ($B_{0,0} = 20$ Pa). Further, trends similar to those shown in Fig. 3 were observed when the next two vertical modes [i.e., the (0,1) and (0,2) modes] were used as sound sources and the number of points in the vertical direction for the G1 grid was doubled.

Four observations are noted from the grid-refinement study in Fig. 3. First, grid G1 is not sufficiently dense for accurate solutions, especially at the lower Mach numbers and higher frequencies (i.e., the reduction in the residual error does not approach the design order). Second, for a fixed Mach number, the reduction in the residual error is smaller at the higher frequencies. A higher grid density is needed to reduce the residual error at higher frequencies. Third, at a fixed frequency, the reduction in the residual error is greater at the higher Mach numbers. This occurs because the convective effect of the flow reduces the axial wave number $K^{+}_{0,0}$ in the rigid-wall duct. Also, the acoustic waves can be resolved on a coarser grid at higher Mach numbers. Fourth, the reductions in the residual error on grids G2 and G4 approach design order (i.e., 16) at each flow Mach number and frequency. Thus, the impedance eduction is performed on the coarser of these two grids (i.e., G2). Similar results to those shown in Fig. 3 were observed when the sound source contained only the (0,1) or the (0,2) mode, but these are not presented here for the sake of brevity.

### 2. *Rigid-Wall Duct Admittance Eductions*

Several examples are now presented to demonstrate the accuracy and robustness of the impedance eduction methodology in rigid-wall ducts that contain planar and higher-order mode sources. Because the impedance of a rigid wall is effectively infinite, the results are presented in terms of the educed normalized admittance, $\beta_2 = 1/\zeta_2$. In these examples, the normalized conductance (i.e., the real part of the normalized admittance) and the normalized susceptance (i.e., the imaginary part of the normalized admittance) of the lower wall are set to a zero value ($\beta_1 = 0.0 + 0.0i$), and the normalized conductance and susceptance of the upper wall are educed. The normalized conductance and susceptance of the upper wall were assumed to be constant to limit the number of design variables. Data for these rigid-wall example studies are simulated from the exact mode solution for outgoing waves in an infinite rigid-wall duct:

$$p(z, x, y) = \sum_{m=0}^{NH-1} \sum_{n=0}^{NV-1} B^{+}_{m,n} e^{iK^{+}_{m,n} z} \cos\left(\frac{n\pi x}{H}\right) \cos\left(\frac{m\pi y}{W}\right) \tag{28}$$

Equation (28) is used to extract the source- and termination-plane acoustic pressures that are required to construct the finite element matrix equation (20)]. Equation (28) also is used to obtain the measured gradients of the acoustic pressure field [see Eqs. (21) and (22)], which are needed to construct the objective function. Only the cuton modes are allowed to propagate through the duct (i.e., $B^{+}_{m,n} =$ 0 Pa for cutoff modes and $B^{+}_{m,n} = 20$ Pa for cuton modes). The

**Table 1 Educed normalized conductance and susceptance of rigid-wall duct at $M_0 = 0.0$ and 0.1**

| | | Plane-wave mode | | (0,1) mode[a] | | Equal amplitude | |
|---|---|---|---|---|---|---|---|
| $f$ | $M_0$ | Conductance | Susceptance | Conductance | Susceptance | Conductance | Susceptance |
| 0.5 | 0.0 | 0.0000 | 0.0000 | N/A | N/A | 0.0000 | 0.0000 |
| 1.0 | 0.0 | 0.0000 | 0.0000 | N/A | N/A | 0.0000 | 0.0000 |
| 1.5 | 0.0 | 0.0000 | 0.0000 | 0.0000 | 0.0000 | 0.0000 | −0.0002 |
| 2.0 | 0.0 | 0.0000 | 0.0000 | 0.0000 | −0.0001 | 0.0000 | −0.0272 |
| 2.5 | 0.0 | 0.0000 | 0.0000 | 0.0000 | −0.0002 | 0.0000 | −0.0003 |
| 3.0 | 0.0 | 0.0000 | 0.0000 | 0.0000 | −0.0005 | 0.0000 | 0.0000 |
| 0.5 | 0.1 | 0.0000 | 0.0000 | N/A | N/A | 0.0000 | 0.0000 |
| 1.0 | 0.1 | 0.0000 | 0.0000 | N/A | N/A | 0.0000 | 0.0000 |
| 1.5 | 0.1 | 0.0000 | 0.0000 | 0.0000 | 0.0000 | 0.0003 | −0.0011 |
| 2.0 | 0.1 | 0.0000 | 0.0000 | 0.0000 | 0.0000 | 0.0009 | −0.0081 |
| 2.5 | 0.1 | 0.0000 | 0.0000 | 0.0000 | 0.0000 | 0.0000 | 0.0000 |
| 3.0 | 0.1 | 0.0000 | 0.0000 | 0.0000 | −0.0001 | 0.0000 | −0.0001 |

[a]N/A denotes that the (0,1) mode is cut off.

**Table 2 Educed normalized conductance and susceptance of rigid-wall duct at $M_0 = 0.3$ and $M_0 = 0.5$**

| | | Plane wave | | (0,1) mode[a] | | Equal amplitude | |
|---|---|---|---|---|---|---|---|
| $f$ | $M_0$ | Conductance | Susceptance | Conductance | Susceptance | Conductance | Susceptance |
| 0.5 | 0.3 | 0.0000 | 0.0000 | N/A | N/A | 0.0000 | 0.0000 |
| 1.0 | 0.3 | 0.0000 | 0.0000 | N/A | N/A | 0.0000 | 0.0000 |
| 1.5 | 0.3 | 0.0000 | 0.0000 | 0.0000 | 0.0000 | 0.0004 | −0.0003 |
| 2.0 | 0.3 | 0.0000 | 0.0000 | 0.0000 | 0.0000 | 0.0003 | −0.0010 |
| 2.5 | 0.3 | 0.0000 | 0.0000 | 0.0000 | −0.0001 | 0.0000 | −0.0002 |
| 3.0 | 0.3 | 0.0000 | 0.0000 | 0.0000 | −0.0002 | 0.0000 | −0.0001 |
| 0.5 | 0.5 | 0.0000 | 0.0000 | N/A | N/A | 0.0000 | 0.0000 |
| 1.0 | 0.5 | 0.0000 | 0.0000 | N/A | N/A | 0.0000 | 0.0000 |
| 1.5 | 0.5 | 0.0000 | 0.0000 | 0.0000 | 0.0000 | 0.0098 | −0.0069 |
| 2.0 | 0.5 | 0.0000 | 0.0000 | 0.0000 | −0.0001 | 0.0000 | −0.0002 |
| 2.5 | 0.5 | 0.0000 | 0.0000 | 0.0000 | −0.0001 | 0.0000 | −0.0003 |
| 3.0 | 0.5 | 0.0000 | 0.0000 | 0.0000 | −0.0001 | 0.0000 | −0.0003 |

[a]N/A denotes that the (0,1) mode is cut off.

**Table 3 Comparison of educed normalized resistance and reactance of test liner at $M_0 = 0.0$ and $M_0 = 0.3$**

| | | Plane wave (GFIT) | | Plane wave (CDTR) | | (0,1) mode (CDTR) | | Equal amplitude (CDTR) | |
|---|---|---|---|---|---|---|---|---|---|
| $f$ | $M_0$ | $\theta_2$ | $\chi_2$ | $\theta_2$ | $\chi_2$ | $\theta_2$ | $\chi_2$ | $\theta_2$ | $\chi_2$ |
| 0.5 | 0.0 | 0.5347 | −2.7893 | 0.5347 | −2.7893 | 0.5347 | −2.7893 | 0.5347 | −2.7893 |
| 1.0 | 0.0 | 0.1984 | −1.1681 | 0.1984 | −1.1681 | 0.1984 | −1.1681 | 0.1984 | −1.1681 |
| 1.5 | 0.0 | 0.2282 | −0.1371 | 0.2282 | −0.1371 | 0.2282 | −0.1371 | 0.2282 | −0.1371 |
| 2.0 | 0.0 | 0.1150 | 0.3469 | 0.1150 | 0.3469 | 0.1150 | 0.3469 | 0.1150 | 0.3469 |
| 2.5 | 0.0 | 0.1598 | 0.6945 | 0.1598 | 0.6945 | 0.1598 | 0.6945 | 0.1598 | 0.6945 |
| 0.5 | 0.3 | 1.7279 | −1.7588 | 1.7279 | −1.7588 | 1.7279 | −1.7588 | 1.7279 | −1.7588 |
| 1.0 | 0.3 | 0.8210 | −0.8741 | 0.8210 | −0.8741 | 0.8210 | −0.8741 | 0.8210 | −0.8741 |
| 1.5 | 0.3 | 0.7517 | −0.3958 | 0.7517 | −0.3958 | 0.7517 | −0.3958 | 0.7517 | −0.3958 |
| 2.0 | 0.3 | 0.7340 | 0.1476 | 0.7340 | 0.1476 | 0.7340 | 0.1476 | 0.7340 | 0.1476 |
| 2.5 | 0.3 | 0.8323 | 0.4356 | 0.8323 | 0.4356 | 0.8323 | 0.4356 | 0.8323 | 0.4356 |

normalized conductance and susceptance values are educed at four Mach numbers for a plane-wave source (i.e., $B^+_{0,0} = 20$ Pa and $B^+_{m,n} = 0$ Pa for $m \neq 0$ and $n \neq 0$), a sound source that contains only the (0,1) mode (i.e., $B^+_{0,1} = 20$ Pa and $B^+_{m,n} = 0$ for $m \neq 0$ and $n \neq 1$), and a sound source that contains equal amplitudes in the first three vertical modes (i.e., $B_{0,0} = B_{0,1} = B_{0,2} = 20$ Pa, $B^+_{0,n} = 0$ Pa for $n \geq 3$ and $B^+_{m,n} = 0$ Pa for $m > 0$).

Table 1 shows the educed normalized conductance and susceptance of the upper wall for $M_0 = 0.0$ and 0.1 for each of the three sound sources. Results for Mach 0.3 and Mach 0.5 are given in Table 2. For each frequency and Mach number, approximately seven iterations and 70 solutions to Eq. (20) with the Pardiso equation solver were needed for the SDFP algorithm to converge to a tolerance of $10^{-8}$ ($\tau = 10^{-8}$). The wall-clock time that was required to converge for each Mach number and frequency was approximately 27 s, and 87 MB of RAM was required on an ALTIX 3700 computer. The first and second columns in Tables 1 and 2 contain the frequency $f$, in kHz, and the uniform-flow Mach number $M_0$, respectively. Because the cuton frequency for the (0,1) mode is 1.5 kHz, the columns that correspond to the educed normalized conductance and susceptance for the (0,1) mode source (i.e., columns five and six in Tables 1 and 2 ) do not contain results below 1.5 kHz. As can be seen in the tables, the normalized conductance and susceptance values that were educed by using the SDFP algorithm are in excellent agreement with their expected value of zero. The educed normalized conductance and susceptance values are observed to be slightly more accurate for the plane-wave source than for the source that contains only the (0,1) mode, whereas the results for the equal mode amplitude source are slightly less accurate than those for the (0,1) mode source.

*3. Soft-Wall Duct Impedance Eductions*

The results in this section test the capability of the proposed impedance eduction methodology to accurately educe the soft-wall impedance at Mach 0.0 and 0.3. The axial pressure gradient that is needed to educe the impedance is obtained as follows:

1) The source- and termination-plane acoustic pressure profiles for the soft-wall duct are set to the same profiles that were used in the rigid-wall example problem.

2) Eq. (20) is then solved by using the liner impedance that was educed in the GFIT to obtain the axial pressure gradients needed for the soft-wall duct impedance eduction [see Eqs. (21) and (22)]. However, the finite element grid that was used to numerically compute

$$\frac{\partial P_s^{\text{Meas}}(0,x)}{\partial z} \qquad \frac{\partial P_e^{\text{Meas}}(L,x)}{\partial z}$$

from Eq. (16) was twice as dense as that used for the impedance eduction. Table 3 compares the educed normalized resistance and reactance values that were obtained with the new method to those educed in the GFIT (using the benchmark method) for each of the three sound sources. The normalized resistance and reactance values are in agreement with the educed values from the benchmark method to five significant digits.

Note also that the small tolerance value that was used in the computer code (i.e., $\tau = 10^{-8}$) was an important contributor to the excellent agreement between the normalized resistance and reactance values educed from the new method and those educed in the GFIT with the benchmark method. For example, Fig. 4 compares the educed resistance and reactance, respectively, for three tolerance

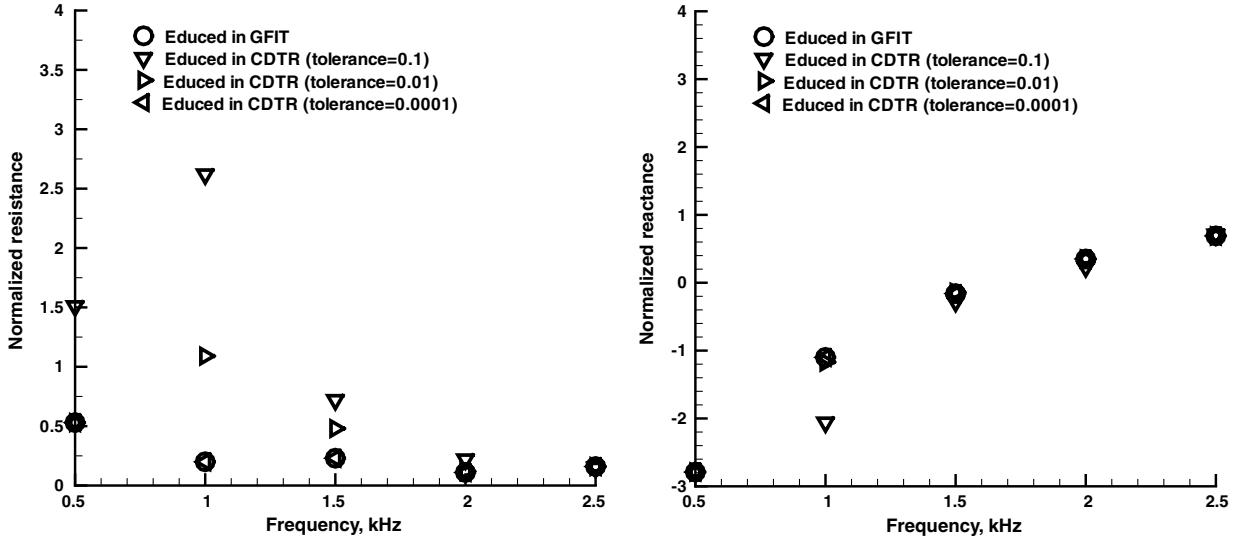


**a) Normalized resistance** **b) Normalized reactance**

**Fig. 4 Effects of optimizer tolerance on educed normalized resistance and reactance of test liner at Mach 0.0 for plane-wave source.**

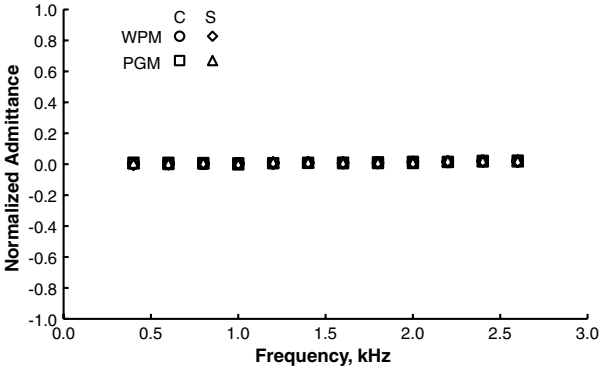


**Fig. 5 Educed normalized admittance, $\beta = C + iS$, of rigid-wall insert for flow-off condition.**

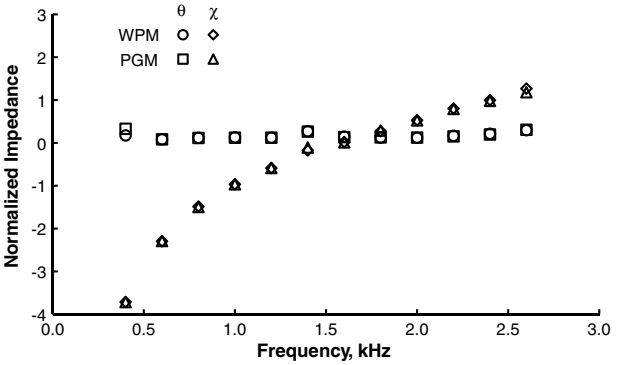


**Fig. 7 Educed normalized impedance, $\zeta = \theta + i\chi$, of conventional liner for flow-off condition.**



values ($\tau = 0.1000$, 0.0100, and 0.0001). The sound source was the plane-wave source, and the Mach number was 0.0. Note that a minimum tolerance of 0.0001 is required for accurate impedance eductions. This minimum tolerance value (i.e., $\tau = 0.0001$) is also required for other Mach numbers, sound sources, and frequencies.

### B. Validation Using Measured Data

Results are now presented for cases in which measured data were used for both a rigid-wall insert and a soft test liner that were inserted into the GFIT. Data were acquired in the GFIT at three flow conditions. For the first flow condition, the flow was off ($M_0 = 0.0$); for the other two flow conditions, the flow was on (i.e., $M_0 = 0.3$ and $M_0 = 0.5$). The Mach number for the flow-on condition is the centerline value. In each example, results from the new impedance eduction method are compared with those produced with the benchmark method. For consistency with a previous paper [37], in the results we refer to the benchmark method as the "wall pressure method" (WPM), because it uses measured acoustic pressures from the lower wall of the GFIT to educe the impedance. The new method is referred to as the "pressure gradient method" (PGM), because it uses the acoustic pressure gradient that is normal to the source- and termination-plane boundaries to educe the impedance.

The GFIT geometry is rectangular with $H = 0.06$ m, $W =$ 0.05 m, $L_1 = 0.20$ m, $L_2 = 0.61$ m, and $L = 1.22$ m (see Fig. 1). For the WPM, measured acoustic pressure data are obtained at 53 unevenly spaced points along the bottom wall. For the PGM, a measurement of the acoustic pressure is taken only at the source and exit planes and at 0.03 m away from these planes (i.e., only four acoustic pressure measurements are required). Because only plane waves are cut on at the frequencies of interest, all acoustic pressure measurements are obtained at the lower rigid wall, and these are assumed to be constant in the vertical direction of the duct (i.e., from the lower wall to the upper wall). The rigid-wall insert is a 12.7-mm-thick stainless-steel plate and is chosen because it provides a liner for which the normalized admittance $\beta_2$ is known (i.e., $\beta_2 = 0.0 + 0.0i$ for a rigid-wall insert). The soft test liner is a single-layer, conventional perforate-over-honeycomb liner. This liner was chosen because it is representative of liners commonly used for the reduction of fan noise in current aircraft engine nacelles. The facesheet for this conventional liner has 0.991-mm-diam holes, an open area ratio of 0.087, and a thickness of 0.635 mm. The depth of the cavity is 38.18 mm; this depth was chosen so that the resonant frequency of the liner is in the middle of the frequency range of interest.

#### 1. *Rigid-Wall Duct Admittance Eductions*

Figure 5 compares the educed normalized conductance and susceptance spectra for the rigid-wall insert for the flow-off condition. Both the WPM and the PGM are in excellent agreement with each other and with the known conductance and susceptance for a rigid-wall insert (i.e., which are known to be zero). Figure 6 shows the comparisons for the two flow-on conditions. The normalized conductance spectra educed with the WPM and the PGM for both flow-on conditions (i.e., $M_0 = 0.3$ and $M_0 = 0.5$) are generally in good agreement with each other. Some scatter can be seen in the susceptance around the expected value of zero for both the WPM and the PGM for the flow-on conditions. Generally speaking, the scatter in the susceptance spectra about the expected value of zero increases with the mean flow Mach number. This result is not surprising when one considers that the refractive effects of the mean boundary layer (which are neglected in both the WPM and the PGM) are more important at higher mean flow Mach numbers.

#### 2. *Soft-Wall Impedance Eductions*

Figure 7 compares the educed normalized resistance and reactance spectra for the conventional liner for the flow-off condition (i.e., $M_0 = 0.0$). Both the resistance and reactance spectra from the WPM and the PGM method are in excellent agreement with each other. Note that the conventional liner is a low-resistance liner for the flow-off condition. Furthermore, for the flow-off condition the resistance

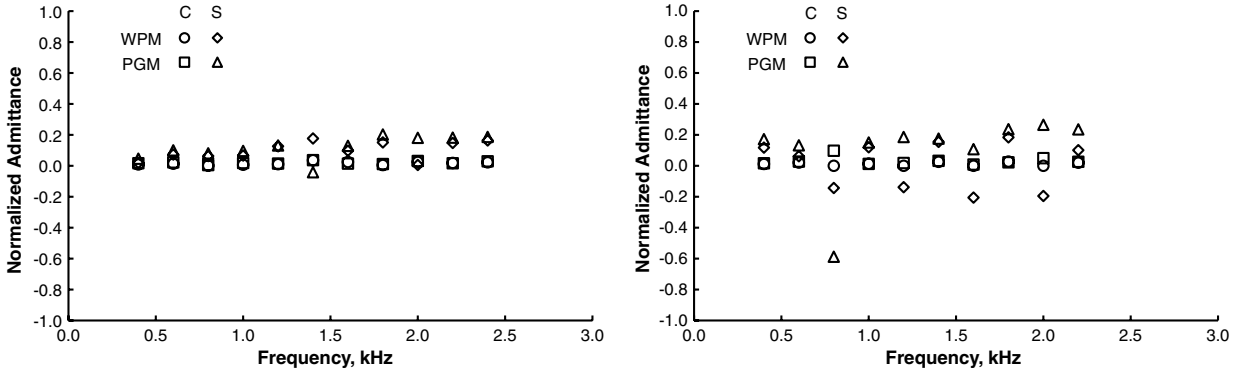


**a) Mach 0.3** **b) Mach 0.5**

**Fig. 6 Educed normalized admittance, $\beta = C + iS$, of rigid-wall insert for flow-on conditions.**

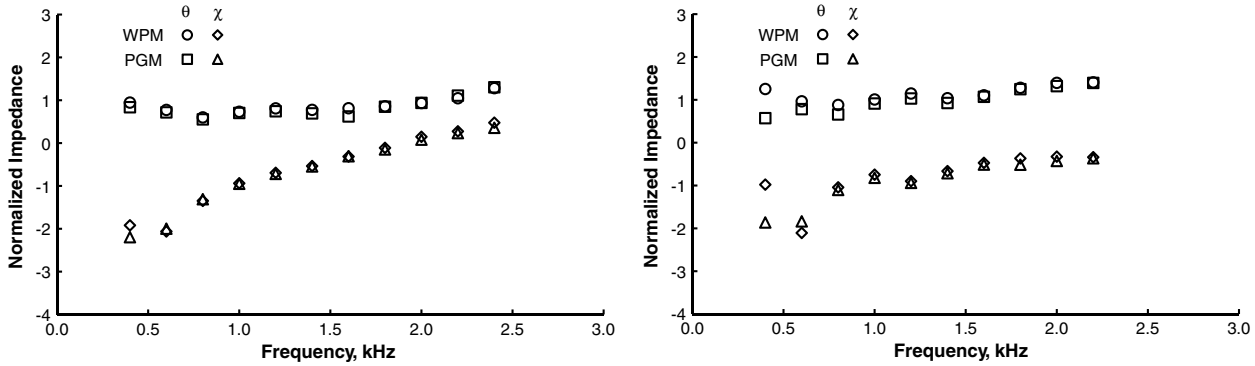


a) Mach 0.3 b) Mach 0.5

**Fig. 8 Educed normalized impedance, $\zeta = \theta + i\chi$, of the conventional liner for flow-on conditions.**



is nearly independent of frequency (as expected), and the normalized reactance follows a $-\cot(kd)$ behavior with the resonant frequency (i.e., the frequency at which the reactance approaches zero) at 1.5 kHz (as expected).

The normalized resistance and reactance spectra educed with the WPM and the PGM for both of the flow-on conditions are depicted in Fig. 8. Educed impedances from both methods (i.e., the WPM and PGM) are in good agreement with each other, especially at the lower Mach numbers. Both eduction methods show an increase in the normalized resistance as the flow Mach number increases (as expected), but the reactance at the low end of each spectra varies from the $-\cot(kd)$ behavior that was observed for the flow-off condition. Some differences also are noted in the educed impedance at the low end of the spectra. These differences were not unexpected and result from the fact that the frequency is approaching an antiresonant value. This result corresponds to previously reported findings in which the reduced attenuation due to an impedance near antiresonance causes the "eye" of the objective function contour to be quite diffuse (i.e., a large range of impedances produces similar attenuations).

**Table 4 Means and standard deviations computed from 121 simulations with WPM and PGM**

| $f$, kHz | $\theta^{\mathrm{WPM}}_{\mathrm{Mean}}$ | $\chi^{\mathrm{WPM}}_{\mathrm{Mean}}$ | $\theta^{\mathrm{PGM}}_{\mathrm{Mean}}$ | $\chi^{\mathrm{PGM}}_{\mathrm{Mean}}$ | $\theta^{\mathrm{WPM}}_{\sigma}$ | $\chi^{\mathrm{WPM}}_{\sigma}$ | $\theta^{\mathrm{PGM}}_{\sigma}$ | $\chi^{\mathrm{PGM}}_{\sigma}$ |
|---|---|---|---|---|---|---|---|---|
| | | | | $M_0 = 0.0$ | | | | |
| 0.4 | 0.17 | −3.71 | 0.33 | −3.72 | 0.13 | 0.07 | 0.32 | 0.76 |
| 0.6 | 0.08 | −2.30 | 0.08 | −2.29 | 0.07 | 0.02 | 0.08 | 0.05 |
| 0.8 | 0.12 | −1.49 | 0.11 | −1.50 | 0.02 | 0.01 | 0.02 | 0.03 |
| 1 | 0.13 | −0.97 | 0.12 | −0.97 | 0.01 | 0.01 | 0.01 | 0.01 |
| 1.2 | 0.12 | −0.59 | 0.12 | −0.59 | 0.00 | 0.00 | 0.00 | 0.00 |
| 1.4 | 0.27 | −0.18 | 0.26 | −0.11 | 0.01 | 0.01 | 0.04 | 0.02 |
| 1.6 | 0.15 | 0.02 | 0.14 | 0.01 | 0.01 | 0.00 | 0.01 | 0.00 |
| 1.8 | 0.12 | 0.27 | 0.13 | 0.29 | 0.01 | 0.00 | 0.01 | 0.01 |
| 2 | 0.12 | 0.53 | 0.12 | 0.52 | 0.03 | 0.01 | 0.03 | 0.01 |
| 2.2 | 0.16 | 0.80 | 0.15 | 0.79 | 0.03 | 0.01 | 0.02 | 0.01 |
| 2.4 | 0.21 | 1.00 | 0.20 | 0.98 | 0.04 | 0.02 | 0.04 | 0.03 |
| 2.6 | 0.30 | 1.27 | 0.31 | 1.18 | 0.07 | 0.03 | 0.08 | 0.04 |
| | | | | $M_0 = 0.3$ | | | | |
| 0.4 | 0.95 | −1.92 | 0.84 | −2.20 | 0.11 | 0.12 | 0.91 | 1.12 |
| 0.6 | 0.77 | −2.06 | 0.72 | −2.00 | 0.07 | 0.09 | 0.40 | 0.36 |
| 0.8 | 0.60 | −1.35 | 0.55 | −1.31 | 0.04 | 0.04 | 0.06 | 0.05 |
| 1 | 0.73 | −0.94 | 0.70 | −0.95 | 0.01 | 0.03 | 0.05 | 0.03 |
| 1.2 | 0.81 | −0.69 | 0.74 | −0.72 | 0.01 | 0.02 | 0.02 | 0.02 |
| 1.4 | 0.78 | −0.54 | 0.69 | −0.55 | 0.01 | 0.01 | 0.06 | 0.03 |
| 1.6 | 0.81 | −0.31 | 0.62 | −0.31 | 0.01 | 0.01 | 0.20 | 0.09 |
| 1.8 | 0.86 | −0.11 | 0.85 | −0.15 | 0.01 | 0.01 | 0.01 | 0.02 |
| 2 | 0.93 | 0.15 | 0.94 | 0.08 | 0.01 | 0.03 | 0.02 | 0.03 |
| 2.2 | 1.05 | 0.27 | 1.11 | 0.23 | 0.01 | 0.02 | 0.02 | 0.03 |
| 2.4 | 1.28 | 0.48 | 1.30 | 0.36 | 0.02 | 0.06 | 0.04 | 0.06 |
| | | | | $M_0 = 0.5$ | | | | |
| 0.4 | 1.25 | −0.98 | 0.57 | −1.86 | 0.08 | 0.14 | 0.51 | 1.07 |
| 0.6 | 0.97 | −2.11 | 0.78 | −1.84 | 0.15 | 0.16 | 0.22 | 0.23 |
| 0.8 | 0.88 | −1.04 | 0.66 | −1.10 | 0.02 | 0.06 | 0.12 | 0.12 |
| 1 | 1.01 | −0.75 | 0.91 | −0.82 | 0.02 | 0.05 | 0.02 | 0.05 |
| 1.2 | 1.15 | −0.90 | 1.03 | −0.94 | 0.02 | 0.05 | 0.05 | 0.06 |
| 1.4 | 1.04 | −0.66 | 0.93 | −0.71 | 0.02 | 0.03 | 0.08 | 0.08 |
| 1.6 | 1.11 | −0.47 | 1.07 | −0.51 | 0.03 | 0.02 | 0.03 | 0.02 |
| 1.8 | 1.28 | −0.37 | 1.25 | −0.52 | 0.04 | 0.01 | 0.04 | 0.03 |
| 2 | 1.40 | −0.33 | 1.32 | −0.43 | 0.04 | 0.02 | 0.04 | 0.02 |
| 2.2 | 1.41 | −0.34 | 1.39 | −0.36 | 0.05 | 0.02 | 0.06 | 0.02 |

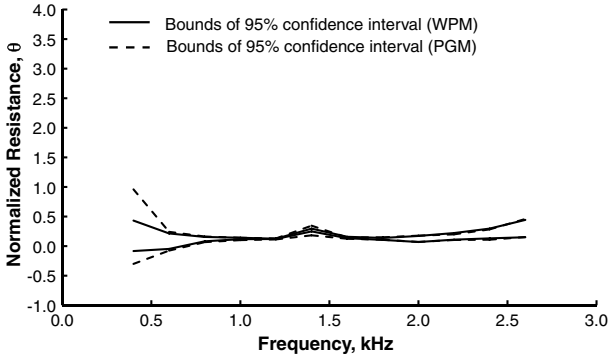


**Fig. 9 The 95% confidence interval for educed normalized resistance for flow-off condition.**

### 3. *Effects of Measurement Uncertainty*

Monte Carlo-type simulations were used to evaluate the uncertainty that is associated with both the WPM and the PGM. For the uncertainty portion of this study, the following steps were followed:

1) For each frequency, the WPM was used to educe the impedance of the conventional liner for the flow-off ($M_0 = 0.0$) and two flow-on ($M_0 = 0.3$ and $M_0 = 0.5$) conditions, based on data that were measured in the NASA LaRC GFIT. The resulting educed impedance, which is considered the baseline for later comparisons, was labeled $\zeta_2^{\mathrm{WPM}} = \theta_2^{\mathrm{WPM}} + i\chi_2^{\mathrm{WPM}}$. The WPM educed impedance spectrum for each of the three flow conditions was then computed to determine $\zeta_2^{\mathrm{WPM}}(M_0, f)$. A similar process was applied using the PGM to educe the impedance spectrum, which is referred to as $\zeta^{\mathrm{PGM}}(M_0, f)$.

2) The measured data were randomly modified (each input value was modified independent of all other input values) within a range of $\pm 0.5$ dB and $\pm 1.0$ deg, and the WPM was used to educe the impedance based on this modified data. The range of variability was chosen to correspond to the maximum possible uncertainty that was expected for this type of microphone. For this portion of the study, the WPM was applied such that

a) A set of 121 simulations (each with a unique set of randomly selected inputs within the selected input range) was completed for each test condition, and the WPM was used to educe the liner impedance. This process resulted in 121 unique impedances at each test condition, which are labeled as $\zeta_l^{\mathrm{WPM}}(M_0, f)$.

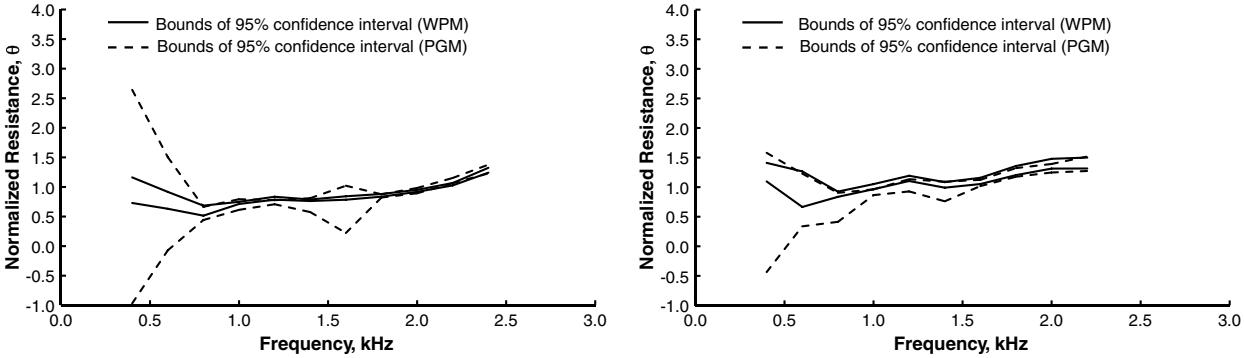


a) Mach 0.3 b) Mach 0.5

**Fig. 10 The 95% confidence interval for educed normalized resistance for flow-on conditions.**

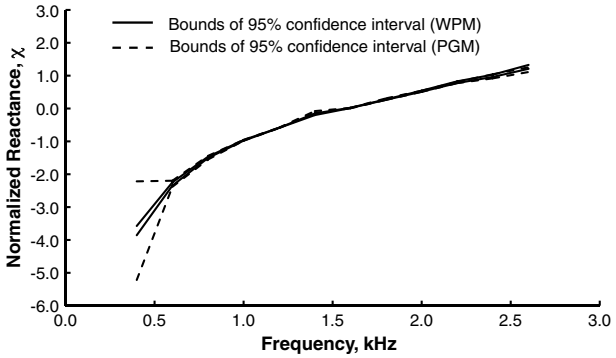


**Fig. 11 The 95% confidence interval for educed normalized reactance for flow-off condition.**

b) The mean, $\zeta_{\text{Mean}}^{\text{WPM}}(M_0, f)$, and standard deviation, $\zeta_{\sigma}^{\text{WPM}}(M_0, f)$, of these 121 educed impedances (at each Mach number and frequency) were computed.

c) A similar process was applied with the PGM to determine $\zeta_{I}^{\text{PGM}}(M_0, f)$, $\zeta_{\text{Mean}}^{\text{PGM}}(M_0, f)$, and $\zeta_{\sigma}^{\text{PGM}}(M_0, f)$.

The means and standard deviations of the impedances that were computed for these 121 simulations were then used to compute the 95% confidence intervals [44] at each test condition. For example, the 95% confidence interval based on the simulations for which the WPM was used is given by

$$\zeta_{\text{CI}}^{\text{WPM}}(M_0, f) = \zeta_{\text{Mean}}^{\text{WPM}}(M_0, f) \pm t_{\text{fac}}\zeta_{\sigma}^{\text{WPM}}(M_0, f)$$

For these 121 simulations, the $t$-factor $t_{\text{fac}}$ takes a value of 1.98. Hence, the user can have 95% confidence that the next simulation conducted with this same approach would provide an impedance that falls somewhere within the specified interval. Table 4 provides the means and standard deviations for the normalized resistance $\theta_2$ and reactance $\chi_2$ educed with both the WPM and the PGM. Clearly, the mean impedance (see Table 4) and the educed impedance without randomization (see Figs. 7 and 8) are in close agreement (as expected).

Figures 9–12 provide additional results for the resistance and reactance uncertainty analysis. Four curves are shown in each of these four figures. The solid curves correspond to the lower and upper bounds of the 95% confidence interval for the WPM, and the two broken curves correspond to those of the PGM. Four general observations are noted from these four figures. First, the difference between the lower and upper bounds of the 95% confidence intervals increases with increasing Mach number for both the WPM and the PGM. This was expected because both the WPM and the PGM assume a uniform mean flow profile instead of the measured shear flow profile. Clearly, the effects of ignoring the shear flow in the propagation model introduces increasing uncertainty as the flow Mach number increases. Second, the height of the confidence intervals for the normalized reactance is smaller than those for the normalized resistance. Therefore, the educed normalized reactance is less sensitive to uncertainty errors than the educed normalized resistance. Third, the uncertainty is generally larger (i.e., the confidence interval is larger) at the low-frequency end of the spectrum; the reason for this discrepancy was discussed in the previous section. Fourth, the uncertainty for the PGM is higher (especially at the low-frequency end of the spectrum) than for the WPM.

We offer a few explanations for why the uncertainty is higher for the PGM than for the WPM. First, the WPM uses 53 input values (i.e., the complex acoustic pressures are measured at 53 microphones on the wall opposite the test liner). The PGM, on the other hand, uses the normal pressure gradients, which are measured at only two points (i.e., the source and exit planes). Second, these normal pressure gradients have been approximated with forward and backward differences at the source and termination planes of the duct, respectively. Therefore, the normal pressure gradient approximations are only

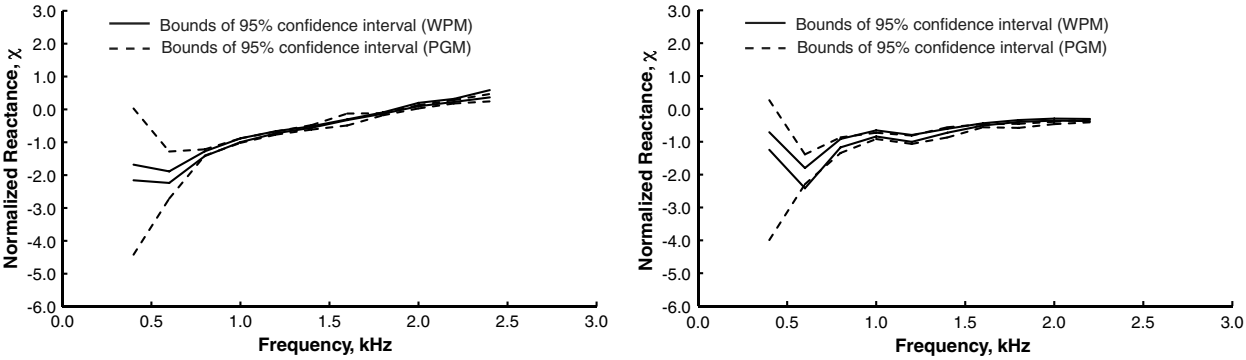


a) Mach 0.3 b) Mach 0.5

**Fig. 12 The 95% confidence interval for educed normalized reactance for flow-on conditions.**

first-order-accurate, whereas the cubic FEM method that is used to solve the Helmholtz equation is fourth-order-accurate. Further, as the flow Mach number increases, the effects of shear also increase, thereby affecting the computation of the normal pressure gradient disproportionately compared with the measured values of the lower-wall pressure that are required for the WPM. Both methods (i.e., the WPM and the PGM) likely would produce better results if a traversing probe were used to measure the complete acoustic pressure profile across the duct at the source and termination planes of the computational domain. Furthermore, this additional input data, along with an improved approximation to the pressure gradients, would cause the PGM uncertainty estimates to track those of the WPM much more closely.

Overall, the uncertainty results presented in this section indicate that the WPM provides a tighter confidence interval than the PGM. This result is further influenced by the antiresonant at the low-frequency end of the spectrum. These results also demonstrate the value of conducting a number of repeatability tests. As the number of tests increases, the confidence interval decreases (i.e., improves), thus justifying the use of the less expensive PGM instead of the WPM.

## VII. Conclusions

A new impedance eduction procedure that extends the capabilities of previously developed impedance eduction techniques has been presented and tested using both simulated and measured data. One issue that may significantly impact the quality of the results that are presented in this paper is the possibility of a hydrodynamic instability in the Myers wall impedance boundary condition. After a careful review of the measured data and the numerical computations, no evidence was found to support the view that the Myers wall impedance boundary condition is generating an instability at the test conditions that are used in this work. Evidence of this instability also has not been reported by the aircraft industry, and no evidence of this instability has been reported in the many laboratory experiments that use the conventional liners that are currently used by the aircraft industry. Based on the results of the current study, the following primary conclusions are drawn:

1) The cubic finite element method that was used in this work converges to the correct solution at the design order. This allows an appropriate grid to be chosen for accurate impedance eduction.

2) The value of the tolerance that is used by Stewart's adaptation of the Davidon–Fletcher–Powell (SDFP) optimization algorithm is an important factor in impedance eduction. Results in this paper show that a minimum value of $10^{-4}$ is needed for this tolerance.

3) When used with simulated data, the new impedance eduction method (as presented in this paper) converges almost exactly to the known impedance of a rigid wall and to that of a known test liner over a range of sound sources, Mach numbers, and source frequencies.

4) When used with measured data, the new impedance eduction method produces results that compare quite favorably with those of the benchmark method. However, at higher Mach numbers, the confidence in the impedance that is obtained with the proposed method is generally not as good as that obtained with the benchmark method. All indications are that this result can be attributed to 1) the neglect of the refractive effects of the mean boundary layer and 2) the disproportionate impact of the error that is introduced by the rather crude approximation to the pressure gradient that is used with the new method (when compared with the impact of the measured lower-wall pressure that is required for the benchmark method).

## References


[1] Taylor, H. O., "A Direct Method of Finding the Value of Materials as Sound Absorbers," *Physical Review*, Vol. 2, No. 4, 1913, pp. 270–287. doi:10.1103/PhysRev.2.270

[2] Seybert, A. F., and Ross, D. F., "Experimental Determination of Acoustic Properties Using a Two-Microphone Random Excitation Technique," *Journal of the Acoustical Society of America*, Vol. 61, No. 5, 1977, pp. 1362–1370. doi:10.1121/1.381403

[3] Chung, J. Y., and Blaser, D. A., "Transfer Function Method of Measuring in-Duct Acoustic Properties, I-Theory, II-Experiment," *Journal of the Acoustical Society of America*, Vol. 68, No. 3, 1980, pp. 907–921. doi:10.1121/1.384778

[4] "Acoustics: Determination of Sound Absorption Coefficient and Impedance in Impedance Tubes, Part 2: Transfer-Function Method," International Organization for Standardization, Std. ISO-10534-2, 1998.

[5] "Standard Test Method for Impedance and Absorption of Acoustical Materials Using a Tube, Two Microphones and Digital Frequency Analysis System," ASTM International, Std. ASTM E1050-98, 2006.

[6] Dean, P., "An *In-Situ* Method of Wall Acoustic Impedance Measurement in Flow Ducts," *Journal of Sound and Vibration*, Vol. 34, No. 1, 1974, pp. 97–130. doi:10.1016/S0022-460X(74)80357-3

[7] Armstrong, D. L., Beckemeyer, R. J., and Olsen, F. R., "Impedance Measurements of Acoustic Duct Liners with Grazing Flow," *Journal of the Acoustical Society of America*, Vol. 55, No. S1, April 1974, p. S59. doi:10.1121/1.1919823

[8] Gallman, J. M., and Kunze, R. K., "Grazing Flow Acoustic Impedance Testing for the NASA AST Program," AIAA Paper 2002-2447, June 2002.

[9] Simonich, J., Narayanan, S., Morin, B., and Patrick, W., "Development and Quantification of an *In-Situ* Grazing Flow Impedance Measurement Technique," AIAA Paper 2005-2848, May 2005.

[10] Jones, M. G., Parrott, T. L., and Watson, W. R., "Comparison of Acoustic Impedance Eduction Techniques for Locally-Reacting Liners," AIAA Paper 2003-3306, May 2003.

[11] Lavieille, M., Simon, F., and Micheli, F., "Measurement of Acoustic Quantity Fields in Duct Flow by Laser Doppler Velocimetry," AIAA Paper 2006-2550, May 2006.

[12] Jones, M. G., Watson, W. R., Parrott, T. L., and Smith, C. D., "Design and Evaluation of Modification to the NASA Langley Flow Impedance Tube," AIAA Paper 2004-2837, May 2004.

[13] Gerhold, C., Cabell, R., and Brown, M., "Development of an Experimental Rig for Investigation of Higher-Order Modes in Ducts," AIAA Paper 2006-2637, May 2006.

[14] Jones, M. G., Watson, W. R., Tracy, M. B., and Parrott, T. L., "Comparison of Two Waveguide Methods for Educing Liner Impedance in Grazing Flow," *AIAA Journal*, Vol. 42, No. 2, 2004, pp. 232–240. doi:10.2514/1.9092

[15] Watson, W. R., "A Method for Determining Acoustic Liner Admittance in a Rectangular Duct with Grazing Flow from Experimental Data," NASA TP-2310, 1974.

[16] Watson, W. R., "A New Method for Determining Acoustic-Liner Admittance in Ducts with Sheared Flow in Two Cross-Sectional Directions," NASA TP-2518, 1985.

[17] Parrott, T. L., Watson, W. R., and Jones, M. G., "Experimental Validation of a Two-Dimensional Shear Flow Model for Determining Acoustic Impedance," NASA TP-2679, 1987.

[18] Watson, W. R., Jones, M. G., Tanner, S. E., and Parrott, T. L., "A Finite Element Propagation Model for Extracting Normal Incidence Impedance In Nonprogressive Acoustic Wave Fields," *Journal of Computational Physics*, Vol. 125, No. 1, April 1996, pp. 177–186. doi:10.1006/jcph.1996.0087

[19] Watson, W. R., Jones, M. G., and Parrott, T. L., "Validation of an Impedance Eduction Method in Flow," *AIAA Journal*, Vol. 37, No. 7, July 1999, pp. 818–824. doi:10.2514/2.7529

[20] Watson, W. R., Tracy, M. B., Jones, M. G., and Parrott, T. L., "Impedance Eduction in the Presence of Shear Flow," AIAA Paper 2001-2236, May 2001.

[21] Watson, W. R., Jones, M. G., Tanner, S. E., and Parrott, T. L., "Validation of a Numerical Method for Extracting Liner Impedance," *AIAA Journal*, Vol. 34, No. 3, March 1996, pp. 548–554. doi:10.2514/3.13102

[22] Watson, W. R., Tanner, S. E., Jones, and Parrott, T. L., "Optimization Method for Educing Variable-Impedance Liner Properties," AIAA Paper 97-1704, June 1997.

[23] Jones, M., Watson, W., and Parrott, T., "Benchmark Data for Evaluation of Aeroacoustic Propagation Codes with Grazing Flow," AIAA Paper 2005-2853, May 2005.

[24] Watson, W. R., Jones, M. G., and Parrott, T. L., "Comparison of a Convected Helmholtz and Euler Model for Impedance Eduction in Flow," AIAA Paper 2006-2643, May 2006.

[25] Watson, W., Jones, M., and Parrott, T., "Investigation of an Anomaly Observed in Impedance Eduction Techniques," AIAA Paper 2008-3013, May 2008.

[26] Eversman, W., and Gallman, J., "Impedance Eduction with an Extended Search Procedure," AIAA Paper 2009-3235, May 2009.
[27] Elnady, T. M., Boden, H., and Elhadidi, B., "Validation of an Inverse Semi-Analytical Technique to Educe Liner Impedance," *AIAA Journal*, Vol. 47, No. 12, Dec. 2009, pp. 2836–2844. doi:10.2514/1.41647
[28] Myers, M. K., "On the Acoustic Boundary Condition in the Presence of Flow," *Journal of Sound and Vibration*, Vol. 71, No. 3, 1980, pp. 429–434. doi:10.1016/0022-460X(80)90424-1
[29] Rienstra, S. W., and Darau, M., "Mean Flow Boundary Layer Effect of Hydrodynamic Instability of Impedance Wall," *Procedia Engineering*, Vol. 6, 2010, pp. 124–132. doi:10.1016/j.proeng.2010.09.014
[30] Marx, D., Auregan, Y., Bailliet, H., and Valiere, J., "PIV and LDV Evidence of Hydrodynamic Instability over a Liner in a Duct with Flow," *Journal of Sound and Vibration*, Vol. 329, No. 18, August 2010, pp. 3798–3812. doi:10.1016/j.jsv.2010.03.025
[31] Syed, A., Yu, J., Kwan, H., and Chien, E., "The Steady Flow Resistance of Perforated Sheet Materials in High Speed Grazing Flows," NASA CR-2002-211749, July 2002.
[32] Auregan, Y., Leroux, M., and Pagneux, V., "Measurement of Liner Impedance with Flow by an Inverse Method," AIAA Paper 2004-2838, May 2004.
[33] Jing, X., Peng, S., and Sun, X., "A Straightforward Method for Wall Impedance Eduction in a Flow Duct," *Journal of the Acoustical Society of America*, Vol. 124, No. 1, July 2008, p. 227. doi:10.1121/1.2932256
[34] Wang, L., Guan, Y., and Wang, T., "The 3-D Modal Method for Acoustic Impedance Determination in Rectangular Duct," AIAA Paper 2008-3015, May 2008.
[35] Taktak, M., Ville, J., Haddar, M., Gabard, G., and Foucart, F., "A 3D Multiport Scattering Matrix Based-Method for Educing Wall Impedance of Cylindrical Lined Ducts Section: Simulation and Error Evaluation," *Advances in Acoustics and Vibration*, Vol. 2009, May 2009, Paper 928367. doi:10.1155/2009/928367
[36] Watson, W. R., and Jones, M. G., "Impedance Eduction in Ducts with Higher-Order Modes and Flow," AIAA Paper 2009-3236, June 2009.
[37] Watson, W. R., and Jones, M. G., "Validation of a New Procedure for Impedance Eduction in Flow," AIAA Paper 2010-3764, June, 2009.
[38] Crocker, M. J., *Handbook of Noise and Vibration Control*, Wiley, Hoboken, NJ, 2007, pp. 131–140.
[39] Desai, C., and Abel, J. F., *Introduction to the Finite Element Method: A Numerical Method for Engineering Analysis*, Van Nostrand Reinhold Company, New York, 1972.
[40] Davidon, W. C., "Variable Metric Methods for Minimization," Argonne National Labs., Rept. ANL-5990, Argonne, IL, 1959.
[41] Fletcher, R., and Powell, M. J. D., "A Rapidly Convergent Descent Method for Minimization," *Computer Journal*, Vol. 6, No. 2, 1963, pp. 163–168.
[42] Stewart, G. W., III, "A Modification of Davidon's Minimization Method to Accept Difference Approximations of Derivatives," *Journal of the Association for Computing Machinery*, Vol. 14, No. 1, 1967, pp. 72–83. doi:10.1145/321371.321377
[43] Goldberg, D., *Genetic Algorithms in Search, Optimization and Machine Learning*, Addison–Wesley, New York, 1989, pp. 75–147.
[44] Coleman, H. W., and Steele, W. G., *Experimentation and Uncertainty Analysis for Engineers*, Wiley, New York, 1989.

J. Astley
*Associate Editor*